ACS PHYSICAL CHEMISTRY Au
AN OPEN ACCESS JOURNAL OF THE AMERICAN CHEMICAL SOCIETY

pubs.acs.org/physchemau

Article

Electron Transfer Dynamics from $CsPbBr_3$ Nanocrystals to Au_{144} Clusters

Kritiman Marjit, Goutam Ghosh, Srijon Ghosh, Debarati Ghosh, Anusri Medda, and Amitava Patra*

Cite This: *ACS Phys. Chem Au* 2023, 3, 348−357

Read Online

ACCESS | Metrics & More | Article Recommendations | Supporting Information

ABSTRACT: Lead halide perovskite nanocrystals have received significant attention as an absorber material for designing efficient optoelectronic devices. The fundamental understanding of the hot carrier (HC) dynamics as well as its extraction in hybrid systems is essential to further boost the performance of solar cells. Herein, we have explored the electron transfer dynamics in the $CsPbBr_3$-Au_{144} cluster hybrid using ultrafast transient absorption spectroscopy. Our analysis reveals faster HC cooling time (from 515 to 334 fs) and a significant drop in HC temperature from 1055 to 860 K in hybrid, suggesting the hot electron transfer from $CsPbBr_3$ nanocrystals to the Au nanoclusters (NCs). Eventually, we observe a much faster hot electron transfer compared to the band-edge electron transfer, and 45% hot-electron transfer efficiency was achieved at 0.64 eV, above band-edge photoexcitation. Furthermore, the significant enhancement of the photocurrent to the dark current ratio in this hybrid system confirms the charge separation via the electron transfer from $CsPbBr_3$ nanocrystals to Au_{144} NCs. These findings on HC dynamics could be beneficial for optoelectronic devices.

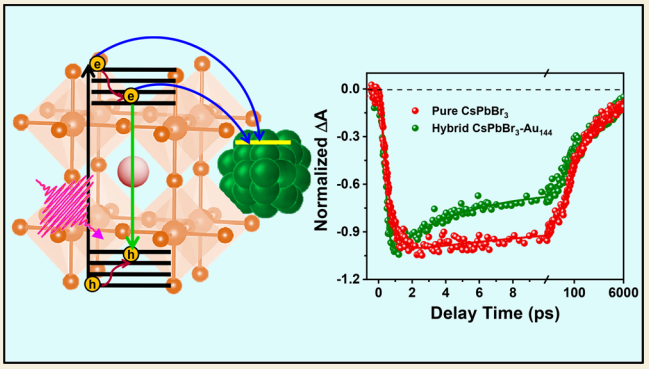

KEYWORDS: *Lead Halide Perovskites, Gold Nanoclusters, Hot Carrier Relaxation, Carrier Extraction, Photocurrent Measurement, Transient Absorption Spectroscopy*

INTRODUCTION

All inorganic lead halide perovskite (LHPs) nanocrystals have received great attention for a variety of optoelectronic applications, such as solar cells,[1−3] photodetectors,[4] and light-emitting diodes,[5] due to their tunable optical properties,[6] longer carrier diffusion length,[7] higher defect tolerant nature,[8] and higher absorption coefficient.[9] To achieve high efficiency in optoelectronic devices, the understanding of the fundamental physical process of photoexcited carriers, i.e, hot carrier (HC) relaxation, ultrafast carrier dynamics, and carrier recombination, in LHPs is very essential.[10−12] In principle, photoexcitation with energy above the bandgap generates the HC in LHPs and its carrier temperature is higher than the lattice temperature. Then, cooling of these HCs occurs by dissipating their excess energy as heat through carrier−carrier and carrier−phonon scattering, which is primarily responsible for the loss of excess energy.[10,11,13,14] The utilization of the excess energy of the HCs through the hot carrier extraction processes can overcome the power conversion efficiency of single-junction solar cells up to 67%, beyond the Shockley−Queisser (SQ) limit.[11,15,16] However, harvesting the excess energy by the HC extraction is highly challenging.

Generally, slow HC cooling in absorber materials and the ability of HC transfer at the interface are two important requirements to realize the efficient extraction of HC.[10,11] The extraction of HCs in conventional semiconductors is limited due to their faster HC cooling processes.[17] Recently, LHPs are recognized with remarkable long-lived HCs, due to various phenomena like hot-phonon bottlenecks,[18] acoustic-optical phonon upconversion,[16] band-filling,[19] and Auger heating processes.[20] Again, the carrier diffusion length of LHPs is sufficiently high to allow the carrier transportation from LHPs surface to energy-selective acceptor materials.[7,21] Recently, there has been growing interest in the HC cooling in lead halide perovskite and many reports have demonstrated slow HC cooling at different excitation energies with varying pump fluence using ultrafast spectroscopy.[7,10,11,22−24] Li et al. successfully demonstrated the efficient HC extraction from $MAPbBr_3$ nanocrystals using Bphen (4,7-diphenyl-1,10-phenanthroline) as an energy-selective hot-electron acceptor and around 83% hot carrier extraction was observed.[25] Recently,

Received: November 30, 2022
Revised: February 15, 2023
Accepted: February 15, 2023
Published: February 28, 2023

we observed 42% hot hole transfer efficiency from $CsPbBr_3$ nanocrystals using surface-anchored porphyrin molecules.[26] Furthermore, a transition metal dichalcogenide and conjugated polymer have been employed to extract the HC from perovskite nanocrystals.[27−29] We investigated the efficient extraction of the hot electrons from $CsPbBr_3$ nanocrystals to the reduced graphene oxide using ultrafast transient absorption spectroscopy.[30] Hayase et al. have used Al_2O_3, poly(3-hexylthiophene-2,5-diyl) (P3HT), and TiO_2 as selective contact materials to extract the HCs from $CsPbI_3$ nanocrystals.[31] Due lack of suitable acceptors and intrinsic competition exists between rapid HC cooling and HC transfer, the extraction of HCs from LHP nanocrystals is still a demanding task. Thus, a systematic study to extract HC with new alternative acceptor materials is important for improving the efficiency of perovskite-based optoelectronic devices.

On the other hand, metal nanoclusters (NCs) are attractive materials due to their ultrasmall size, high photostability, and tunable luminescence properties with the varying number of atoms and ligands.[32,33] Besides, NCs have gained great success as energy selective acceptor materials and materials for interface modification, and they couple excellently with quantum dots.[34−37] We have demonstrated the ultrafast charge transfer from CdSe nanoplatelets to Au_{25} NCs.[38] Recently, Au_{144} NCs have emerged as promising NCs because they exhibit the electronic characteristic in between the molecular and metallic behavior.[39−41] Therefore, forming a hybrid of LHPs with Au_{144} NCs can be an effective strategy that can be employed to improve the efficiency of optoelectronic devices.

Herein, we have investigated the ultrafast carrier dynamics of hybrid $CsPbBr_3$-Au_{144} to understand the carrier extraction process using ultrafast transient absorption spectroscopy (TAS). The faster HC cooling dynamics and reduction of initial HC temperature (T_C) in hybrid $CsPbBr_3$-Au_{144} confirm the hot electron transfer from $CsPbBr_3$ nanocrystals to Au_{144} NCs. Furthermore, the hybrid system exhibits an enhanced photocurrent and higher photocurrent-to-dark current ratio compared to that of pure $CsPbBr_3$ nanocrystals. The overall results of our work suggest that charge separation occurs in the hybrid system via electron transfer from $CsPbBr_3$ nanocrystals using Au_{144} NCs. Our study will pave the way for the development of new-generation optoelectronics devices.

EXPERIMENTAL SECTION

Materials

Cesium carbonate (Cs_2CO_3), lead bromide ($PbBr_2$), 1-octadecene-(ODE), oleic acid (OA), and oleylamine (OLAM) were purchased from Sigma-Aldrich and used without any further purification. Tetrachloroauric acid ($HAuCl_4{\cdot}3H_2O$) was purchased from Sigma-Aldrich. Sodium borohydride ($NaBH_4$), sodium hydroxide (NaOH), tetraoctyl ammonium bromide (TOABr), and 2-phenylethanethiol (PhC_2H_4SH, 99%) were purchased from Merck India Ltd. Methyl acetate (MeOAC, Merck) was used during the purification of the nanocrystals. Solvents like toluene, ethanol, methanol, acetonitrile, and dichloromethane were obtained from Spectrochem. Toluene (Spectrochem) was used for all spectroscopic experiments, including the characterization of the nanocrystals.

Synthesis of $CsPbBr_3$ Nanocrystals

$CsPbBr_3$ nanocrystals are synthesized following the previously reported hot injection method with some minor modifications.[6] Preparation of Cs-oleate: Briefly, Cs_2CO_3 (0.25 mmol) was taken in a 25 mL two-neck flask along with 8 mL of octadecene and 0.5 mL of OA. The solution was kept under vacuum for 1h at 120 °C and then heated to 150 °C under N_2 until all Cs_2CO_3 dissolved. After the formation of a clear solution, the solution temperature was maintained at 100 °C to avoid precipitation of Cs-oleate. In a separate 25 mL two-neck flask, 0.18 mmol $PbBr_2$ and 1-octadecene (5 mL, ODE) were taken and dried under vacuum for 1 h at 120 °C with continuous stirring. Then, 0.5 mL of dried OA and 0.5 mL of dried OLAM were injected into the solution at 120 °C under an N_2 atmosphere. The temperature was increased to 170 °C after the complete solubilization of $PbBr_2$ salt. Then, 0.4 mL of Cs-oleate solution (as described above) was quickly injected, and an ice−water bath immediately cooled the reaction mixture. The crude solution was precipitated out by methyl acetate (MeOAC) and separated by centrifuging at 7500 rpm for 7 min. The supernatants were discarded, and the residues were redispersed in toluene for further characterization.

Synthesis of $Au_{144}(SC_2H_4Ph)_{60}$ NCs

Au_{144} NCs were prepared followed by an earlier reported method.[42] In a typical synthesis, $HAuCl_4{\cdot}3H_2O$ (0.3 mmol, 118 mg) and TOABr (0.348 mmol, 190 mg) were added to a 50 mL trineck round-bottom flask and mixed with 15 mL of methanol. After being vigorously stirred for 15 min, the solution color was changed from yellow to dark red. Then, C_2H_4PhSH (1.59 mmol) was added to the solution at room temperature. Then, the color of the reaction mixture rapidly turned white. After ∼15 min, a fresh $NaBH_4$ solution (3 mmol, dissolved in 6 mL of cold Milli-Q water) was rapidly added to the solution under vigorous stirring. The color of the solution immediately turned black and produced Au NCs, which were precipitated out of the methanol solution. The reaction was stopped after ∼5 h, and the black precipitate was collected by centrifugation (5 min at ∼5000 rpm). The black precipitates were washed with excess methanol and collected by centrifugation again. This step was repeated at least 3 times to completely remove the free thiol residue. Then, toluene was used to separate the Au NCs from Au(I)-SR polymers. Next, the as-obtained Au NCs were washed with acetone. Finally, the crude product was separated by centrifugation, and $Au_{144}(SC_2H_4Ph)_{60}$ NCs were obtained as the black precipitate. $Au_{144}(SC_2H_4Ph)_{60}$ NCs were dispersed in toluene. The MALDI mass spectra of the as-synthesized $Au_{144}(SC_2H_4Ph)_{60}$ NCs are provided in figure S1.

Preparation of $CsPbBr_3$-Au_{144} Hybrid

The $CsPbBr_3$ nanocrystal solution was dispersed in toluene and the band-edge optical density (OD) was kept fixed at 0.1. Then, the OD of the synthesized Au_{144} NCs was also fixed at 0.07 at 420 nm in toluene. Au_{144} NCs solution was added to the $CsPbBr_3$ nanocrystals solution, followed by ultrasonication for 5 min. Then, this solution mixture was kept for about 2 h in an inert atmosphere with constant stirring. After the formation of the hybrid, all morphological, optical, and other spectroscopic and photovoltaic characterizations were carried out.

Characterization

Transmission Electron Microscopy. The transmission electron microscopy (TEM) images are taken from a JEOL JEM-2100F at an operating voltage of 200 kV. The samples have been drop-casted on a carbon-coated copper grid.

Powder X-ray Diffraction. We performed X-ray diffraction (XRD) using Cu Kα source (1.5418 Å) radiation (Bruker D8 Advance).

Steady-state UV−Vis Absorption and Photoluminescence (PL). We conducted the absorption and emission studies using a UV−vis spectrophotometer (Shimadzu) and a Fluoromax-P instrument (Horiba JOBIN YVON), respectively.

Time-Correlated Single Photon Counting Measurements. Time-correlated single-photon counting (TCSPC) has been performed for photoluminescence decay time measurements. Radiation of 400 nm with a picosecond NANO-LED IBH 375L instrument was used to excite the samples. The typical full width at half-maximum (fwhm) of the system response using liquid scatters was ∼90 ps. The repetition rate is 1 MHz. The fluorescence decay was analyzed by

https://doi.org/10.1021/acsphyschemau.2c00070
ACS Phys. Chem Au 2023, 3, 348−357

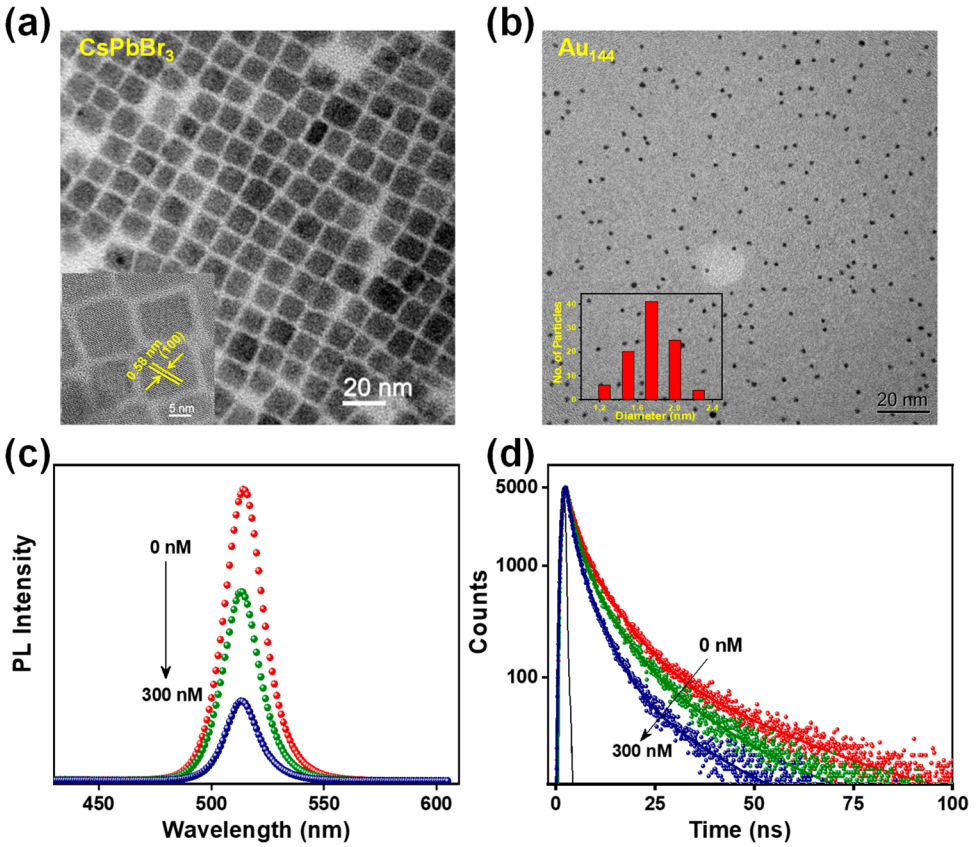

Figure 1. TEM images of (a) pure $CsPbBr_3$ nanocrystals (inset shows HRTEM images) and (b) pure Au_{144} NCs (inset show size distribution). Photoluminescence (c) quenching and (d) decay curves of pure $CsPbBr_3$ nanocrystals with the gradual addition of Au_{144} NCs concentration [λ_{ex} = 371 nm and λ_{em} = 515 nm].

using IBH DAS6 software. To analyze the time-resolved fluorescence decay, we have the following equation.[43]

$$P(t) = b + \sum_{i}^{n} \alpha_i \exp\left(-\frac{t}{\tau_i}\right) \quad (1)$$

where n and b are the number of discrete emissive species and a baseline correction ("dc" offset), respectively. α_i and τ_i are the pre-exponential factors and excited-state fluorescence lifetimes associated with the ith component, respectively. For multiexponential decays, the average lifetime, $\langle\tau\rangle$, is estimated using the equation:

$$\langle\tau\rangle = \sum_{i=1}^{n} \beta_i \tau_i \quad (2)$$

Here, $\beta_i = \alpha_i/\Sigma\alpha_i$ is the contribution of the decay component. Also, α_i and τ_i indicate the pre-exponential factors and excited state fluorescence lifetimes associated with the ith component, respectively.

Ultrafast Transient Absorption Measurements. Femtosecond transient absorption (fs-TA) measurements have been performed using a 400 nm pump pulse with 120 fs duration. The subsequent excited-state dynamics have probed with a white-light continuum (WLC) of the entire visible region. To avoid sample degradation and the multiexciton effect, we have kept low the pump power (<5 $\mu J/cm^2$). We have analyzed the data using the Surface Xplorer version 4.0 software, and group velocity dispersion (GVD) are removed by chirp correction using the same software. Detailed instrumental descriptions of the TA setup were described in our previous reports.[44] Briefly, a pulse (<100 fs duration, 80 MHz repetition rate, with 800 nm wavelength) was created by a mode-locked Ti: sapphire oscillator (Seed laser, Mai-Tai SP, Spectra-Physics). These seed pulses are amplified by a separate pump laser (Nd: YLF laser, 527 nm, ASCEND EX, Spectra-Physics). The Spitfire Ace amplifier's output (800 nm, <100 fs, 1 kHz, pulse energy 5 mJ) was sent to the spectrophotometer. This output was divided into two parts: one part was used to generate a 400 nm pump beam by the BBO crystal, and the other amount of the 800 nm light was focused on a CaF_2 crystal to develop a white-light continuum (WLC). The instrument response function of our TA instruments is 120 fs.

Device Fabrication. For the fabrication of $CsPbBr_3$ nanocrystals and $CsPbBr_3$-Au_{144} hybrid device, we have taken patterned ITO substrates. ITO substrates were cleaned by sonication in various solvents like a mixture of distilled water and detergent solution, Milli-Q water, acetone, absolute alcohol, and isopropyl alcohol for 10 min each. Next, the substrates were purged with argon gas for 7 min for each device. Then, poly(3,4-ethylene dioxythiophene):polystyrenesulfonate (PEDOT:PSS) solution was spin-coated on ITO-covered substrates at 2500 rpm for 30 s, and it was heated at around 60 °C for 1 h in the vacuum chamber. After that, the substrates were spin-coated for the deposition of each layer. First, we took $CsPbBr_3$ nanocrystals dissolved in toluene with a concentration of 20 mg/mL, spin-coated them at 2000 rpm for 30 s, then dried them at 50 °C. On the other hand, hybrid $CsPbBr_3$-Au_{144} was spin-coated following the above methods. We took more concentrated samples than those that were used for spectroscopic characterization. Afterward, the substrates were placed into a vacuum chamber for the thermal evaporation of a 100 nm thick Al cathode layer through a shadow mask. The devices were put inside the vacuum after the deposition of the metal contact layer. Finally, the measurements were performed using the active area of devices determined from the overlap of ITO and Al. Photocurrent measurement was conducted using a solar simulator equipped with a 300 W xenon lamp (power supply Newport model 69911) with white light under 1 sun (AM 1.5 G) illumination at 100 mW cm^{-2}.[38]

Cyclic Voltammetry Measurement. Cyclic voltammetry (CV) measurements have been performed using a PC-controlled P.A.R. model 273A. We have used a Pt wire working electrode, a Pt counter

https://doi.org/10.1021/acsphyschemau.2c00070
ACS Phys. Chem Au 2023, 3, 348−357

electrode, and an Ag/Ag+ reference electrode in toluene containing 0.1 M TBAP as the supporting electrolyte. A ferrocene/ferrocenium redox couple has been used as an internal standard. Detailed calculations of the valence band (VB) and conduction band (CB) position can be found elsewhere.[38,45]

RESULTS AND DISCUSSION

Structural Analysis

We have prepared pure $CsPbBr_3$ nanocrystals via a hot-injection protocol (details in the Experimental Section).[6] TEM images of the as-synthesized nanocrystals show a highly monodispersed cubic shape with an average edge length of 12.5 ± 0.5 nm (Figure 1a). Notably, the synthesized nanocrystals are larger than the exciton Bohr radii of $CsPbBr_3$ nanocrystals and exhibit a weak quantum confinement effect.[46] Additionally, high-resolution transmission electron microscopy (HRTEM) images are provided in the inset of Figure 1a, which reveals an interplanar distance of 0.58 nm corresponding to the (100) lattice plane. Figure 1b presents a highly monodispersed and spherical morphology of pure Au_{144} NCs with 1.8 ± 0.2 nm average sizes.[47] Furthermore, the TEM image of hybrid $CsPbBr_3$-Au_{144} (Figure S2) indicates that Au_{144} NCs are attached with $CsPbBr_3$ nanocrystals and the morphology of both $CsPbBr_3$ nanocrystals and Au_{144} NCs does not change after the formation of the hybrid structure. The HRTEM image of the hybrid is shown in the inset of Figure S2, and interestingly, it exhibits an unaltered interplanar distance (~0.58 nm) corresponding to the (100) lattice plane compared to that of pure $CsPbBr_3$ nanocrystals. Again, the powder XRD pattern of the pure $CsPbBr_3$ nanocrystals and hybrid $CsPbBr_3$-Au_{144} is presented in Figure S3. The XRD pattern of pure $CsPbBr_3$ nanocrystals informs it is a cubic crystal phase.[48] Additionally, we observe that the XRD pattern of hybrid $CsPbBr_3$-Au_{144} does not exhibit minimal peak shift compared to pure $CsPbBr_3$ nanocrystals, which indicates no change in the crystal structure of $CsPbBr_3$ nanocrystals due to the formation of hybrid structure.

Steady-State and Time-Resolved Spectroscopy

The normalized UV−vis absorption and photoluminescence (PL) spectra of $CsPbBr_3$ nanocrystals are presented in Figure S4a. The first excitonic transition in the absorption band (dotted lines) is observed at 504 nm, and the corresponding sharp PL bands (solid lines) for band edge emission evolve at 515 nm. Figure S4b depicts the absorbance bands of as-synthesized Au_{144} NCs. The Au_{144} NCs display absorption bands at 336, 463, 517, and 700 nm due to electronic transition in the NCs, which agrees with the previous report.[33,47] Furthermore, we have performed the steady-state absorption and photoluminescence experiment of both pure $CsPbBr_3$ nanocrystals and hybrid $CsPbBr_3$-Au_{144} system. Figure S4c presents the UV−vis absorption spectra of pure $CsPbBr_3$ nanocrystals and hybrid $CsPbBr_3$-Au_{144} system, which show additive spectral features that indicate no ground-state interaction occurs between $CsPbBr_3$ nanocrystals and Au_{144} NCs. Figure 1c displays the PL spectra of $CsPbBr_3$ nanocrystals (fixed concentration, 40 nM) with the increasing amount of Au NCs (0−300 nM) at 400 nm excitation. Interestingly, we observe that the intensity of band edge emission of $CsPbBr_3$ nanocrystals (i.e., 515 nm) drastically decreases up to 70% upon the addition of 300 nM Au_{144} NCs. Next, the TCSPC experiments are carried out to investigate the excited state interaction in the hybrid system. All of the samples are excited at 371 nm, and the emission decay is monitored at the band-edge emission position (515 nm). Figure 1d shows that the PL decay of pure $CsPbBr_3$ nanocrystals gradually becomes faster with the increase of the amount of Au_{144} NCs (up to 300 nM). Interestingly, it is found that the average lifetime of pure $CsPbBr_3$ nanocrystals is decreased from 5.8 ± 0.2 to 1.6 ± 0.3 ns in the presence of 300 nM Au_{144} NCs. Here, the PL decay curves are fitted triexponentially (Table S1). The fitted decay components for pure $CsPbBr_3$ nanocrystals along with their contributions are as follows: τ_1 = 1.5 ns (56%), τ_2 = 6.2 ns (34%), and τ_3 = 29.1 ns (10%). Whereas the decay components of the hybrid system with their respective contribution are as follows: τ_1 = 0.8 ns (84%), τ_2 = 2.3 ns (12%), and τ_3 = 16 ns (4%). It is well documented that τ_2, the intermediate time component, arises for excitonic recombination, and the other two components (τ_1 and τ_3) arise due to the carrier trapping mediated processes.[12,49] Here, we observe that the value of the faster time decreases with an enhanced contribution in the case of the hybrid system, indicating additional nonradiative deactivation pathways. Therefore, we can conclude that the drastic PL quenching and the shortening of the average decay time of pure $CsPbBr_3$ nanocrystals in the hybrid system occur either due to charge transfer (electron/hole) or energy transfer. Here, we neglect the possibility of the energy transfer process because there is no efficient spectral overlap between the absorption spectrum of Au_{144} NCs and the emission spectrum of $CsPbBr_3$ nanocrystals. Furthermore, for the electron or hole transfer process, we have analyzed the band alignment of pure $CsPbBr_3$ nanocrystals and the Au_{144} NCs (shown in Figure 2).

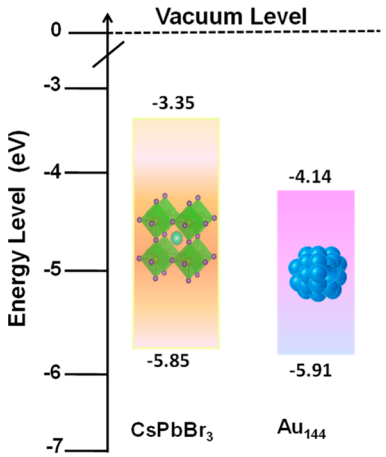

Figure 2. Schematic energy level diagram of $CsPbBr_3$ nanocrystals and Au_{144} NCs.

The band position of Au_{144} NCs is estimated from a cyclic voltammetric (CV) study, which is in close agreement with previous results (Figure S5).[37,38] The band energy of pure $CsPbBr_3$ nanocrystals has been obtained from previous reports.[50] The alignment of energy levels indicates that electron transfer from pure $CsPbBr_3$ nanocrystals to Au_{144} NCs is thermodynamically feasible in a hybrid system.

Ultrafast Carrier Dynamics

We have performed femtosecond TAS to unravel the ultrafast carrier dynamics of both pure $CsPbBr_3$ nanocrystals and hybrid systems. All the fs-TAS measurements have been performed at 400 nm excitation with low pump fluence (~5 $\mu J/cm^2$) to

https://doi.org/10.1021/acsphyschemau.2c00070
ACS Phys. Chem Au 2023, 3, 348−357

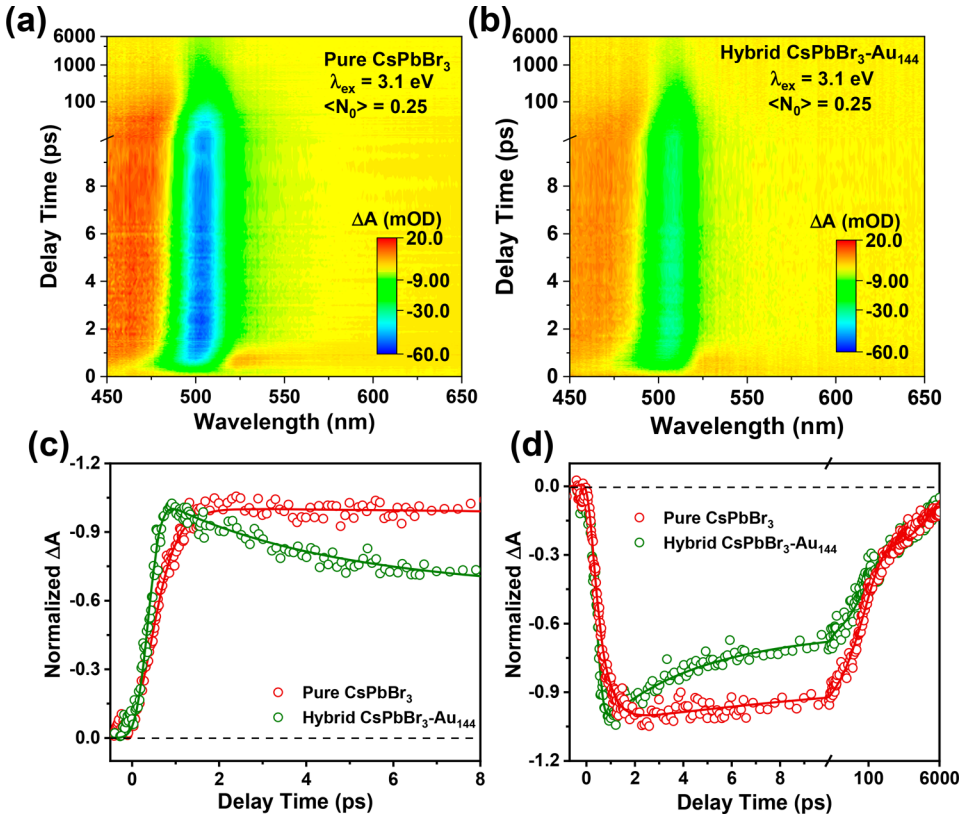

Figure 3. Two-dimensional pseudocolor TA map of (a) pure $CsPbBr_3$ nanocrystals and (b) hybrid $CsPbBr_3$-Au_{144}. Comparison of (c) bleach formation kinetics and (d) ground state bleach recovery dynamics of pure $CsPbBr_3$ nanocrystals and hybrid $CsPbBr_3$-Au_{144} system [λ_{ex} = 400 nm].

avoid multiphoton absorption. The average number of exciton per nanocrystals ($\langle N_0 \rangle$) is calculated to be 0.25.[30] Figure 3a,b shows the 2D pseudocolor TA map of pure $CsPbBr_3$ nanocrystals and hybrid $CsPbBr_3$-Au_{144} system, respectively. Again, Figure S6 presents the time evolution of the corresponding TA spectra of the samples. The spectral characteristics of both the samples are (i) a strong negative ground state bleach signal (GSB) at around the bandgap (505 nm) which arises for the state filling effect,[24,51,52] (ii) a short-lived positive photoinduced absorption (PIA) at the lower-energy side of the first excitonic band (530−575 nm) due to bandgap renormalization process, and (iii) a long-lived PIA at the higher-energy side of the bleach (450−470 nm) due to absorption of the carrier at band-edge state.[16,53,54] Notably, a derivative-like spectral feature at early delay times arises due to the Columbic interaction between the hot excitons and band edge excitons, generated by the pump and probe laser, respectively. This is known as the biexciton-induced stark effect and is responsible for the redshift of the GSB signal.[55−57] Again, the initial intensity of the GSB signal of both samples increases and reaches a maximum at early delay times because a short-lived positive PIA signal is replaced by a strong GSB signal after the relaxation of hot carriers to the lowest-energy band edge states.[26] Here, we observe that the amplitude of GSB bleach of pure $CsPbBr_3$ nanocrystals decreases significantly in the hybrid $CsPbBr_3$-Au_{144} system (Figure 3a,b). This suggests that the depopulation of excited carriers occurs from $CsPbBr_3$ nanocrystals to surface-attached Au_{144} NCs. Again, careful observation of the magnified TA spectra (Figure S6b) in the hybrid system suggests that there is a broad PIA signal at around the 565−675 nm range for the hybrid system. According to the previous reports, this PIA signal arises for the formation of Au_{144}^{-}.[41] It is noted that we have used a very low concentration (300 nM) of Au_{144} NCs to form the hybrid to eliminate the influence of Au_{144} NCs in the TA signal. Figure S7 confirms that the same concentration (used for the hybrid $CsPbBr_3$-Au_{144} system) of pure Au_{144} NCs does not exhibit a significant TA signal at 400 nm excitation. Thus, the combined results of the reduction of GSB amplitude and the formation of the Au_{144}^{-} in a hybrid system indicates that the electron transfer occurs from $CsPbBr_3$ nanocrystals to Au_{144} NCs.

It is well established that the HC cooling time is reflected as the build-up time (growth time) of the GSB signal.[12,16] The rise (growth) time represents the average relaxation time of both carriers (electron and hole) because LHPs nanocrystals have a comparable effective mass of an electron and hole.[6] Figure 3c represents the comparison of the growth time between pure $CsPbBr_3$ nanocrystals and the hybrid $CsPbBr_3$-Au_{144} system. We observe the faster growth time in the hybrid system (334 ± 15 fs) compared to the pure one (515 ± 12 fs), indicating hot-carrier transfer occurs from pure $CsPbBr_3$ nanocrystals to attached Au_{144} NCs. Notably, the growth of the GSB and the decay of short-lived PIA decay are concomitant and both arise due to the carriers arriving at the band edge after the initial thermalization and relaxation process.[24,26] Figure S8 represents the overlap between short-lived PIA decay and GSB growth dynamics of pure $CsPbBr_3$ nanocrystals and hybrid $CsPbBr_3$-Au_{144} system. We have performed the global fitting (details shown in the SI) of the TA spectra employing a two-component sequential decay model to determine the HC relaxation time (Figure S9).[26] The obtained HC cooling time for the pure $CsPbBr_3$ nanocrystals and hybrid $CsPbBr_3$-Au_{144} system are 515 ± 20 and 334 ± 15

https://doi.org/10.1021/acsphyschemau.2c00070
ACS Phys. Chem Au 2023, 3, 348−357

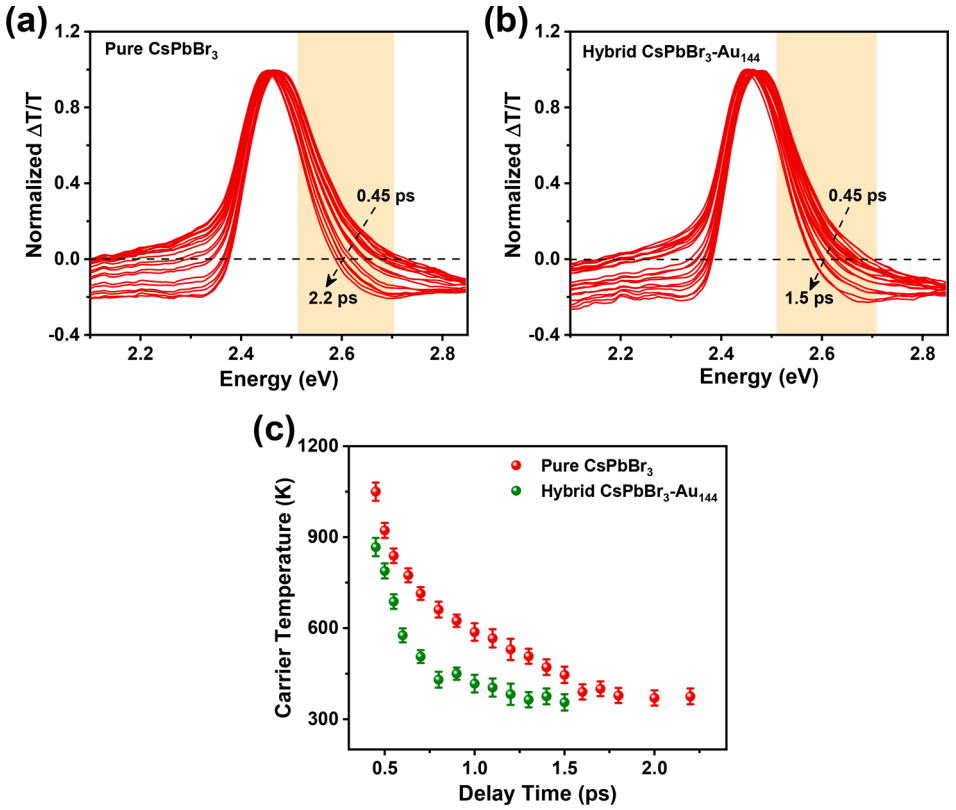

Figure 4. Normalized TA spectra of (a) pure $CsPbBr_3$ nanocrystals and (b) hybrid $CsPbBr_3$-Au_{144}. (c) Transient evolution of the carrier temperature for pure $CsPbBr_3$ nanocrystals and hybrid $CsPbBr_3$-Au_{144} system (error bar represents the standard deviation. [λ_{ex} = 400 nm].

fs, respectively. Notably, the origin of the faster HC relaxation may also arise due to the coupling of the carrier with surface-related defect/trap states.[25,57] The photoluminescence excitation (PLE) spectra closely match the absorption spectra for both samples (Figure S10), indicating that almost all HCs are effectively funneled to the emitting band-edge states.[24] Hence, the faster HC relaxation in the hybrid system occurs due to hot electron transfer from $CsPbBr_3$ nanocrystal to Au NCs, not due to the surface-related defect/trap states. Besides, we have estimated the hot electron transfer rate by the following equation.[58]

$$k_{\text{hot-electron}} = \frac{1}{\tau^{\text{growth}}_{\text{hybrid}}} - \frac{1}{\tau^{\text{growth}}_{\text{CsPbBr3}}} \quad (3)$$

The calculated hot-electron transfer rate from $CsPbBr_3$ nanocrystals to Au_{144} NCs in a hybrid system is 1.05×10^{12} s^{-1}. Furthermore, we have calculated the hot electron transfer efficiency by monitoring the absolute bleach amplitude of the samples at early delay times (Figure S11). Interestingly, the significantly reduced amplitude suggests the transfer of hot electrons from pure $CsPbBr_3$ nanocrystals to Au_{144} NCs, and the hot electron transfer efficiency is 45%. Next, the "cold electron" (i.e., band-edge electron) transfer dynamics have been investigated by monitoring the ground state bleach recovery dynamics. Figure 3d depicts the comparison of bleach recovery dynamics of pure $CsPbBr_3$ nanocrystals and the hybrid $CsPbBr_3$-Au_{144} system. The fitted decay components are shown in Table S2. Here, the bleaching kinetics of pure $CsPbBr_3$ nanocrystals is fitted biexponentially with decay time constants of 60 ± 9 ps (65%) and >1 ns (35%). According to the previous reports, the longer component arises due to the radiative recombination of electron and hole, and the shorter component originates from the trap state mediated process.[12,59] The GSB kinetics of hybrid $CsPbBr_3$-Au_{144} is fitted well with three decays time constants: 1.8 ± 0.3 ps (70%), 37 ± 5 ps (19%), and >1 ns (11%). The careful observation of the decay parameters suggests that the additional faster component with the enhanced contribution in the hybrid system arises due to the transfer of band-edge electrons from $CsPbBr_3$ nanocrystals to attached Au_{144} NCs. Therefore, a hybrid system exhibits a much faster bleach recovery compared to a pure one. Then, the estimated band-edge electron transfer rate is 5.56×10^{11} s^{-1}. We observe that the hot electron transfer rate is almost two times faster than the band-edge electron transfer rate in the presence of Au_{144} NCs.

To examine the HC cooling dynamics more carefully, we have monitored the transient evolution of HC temperature (T_C), which enables us to visualize the HC extraction process in the hybrid system. Figure 4 (a and b) displays the normalized $\Delta T/T$ TA spectra of pure $CsPbBr_3$ nanocrystals and hybrid $CsPbBr_3$-Au_{144}, respectively. The shaded region of Figure 4a and b represents the high energy tails of the GSB signal, which signifies the energy distribution of state fillings by HCs. Notably, This high energy tail arises from the rapid distribution of the initially created nonequilibrium carriers population into quasi-equilibrium Fermi–Dirac distribution through the carrier–carrier scattering process within 100 fs.[24] Generally, the T_C is much larger than the lattice temperature (T_L), and it equilibrates with the lattice through inelastic carrier-phonon scattering.[19,25,60] Hence, the Fermi–Dirac distribution function can be approximated by a Maxwell–Boltzmann distribution function at the high energy tails. Thus, T_C is estimated by fitting the high energy tail of the GSB signal

https://doi.org/10.1021/acsphyschemau.2c00070
ACS Phys. Chem Au 2023, 3, 348–357

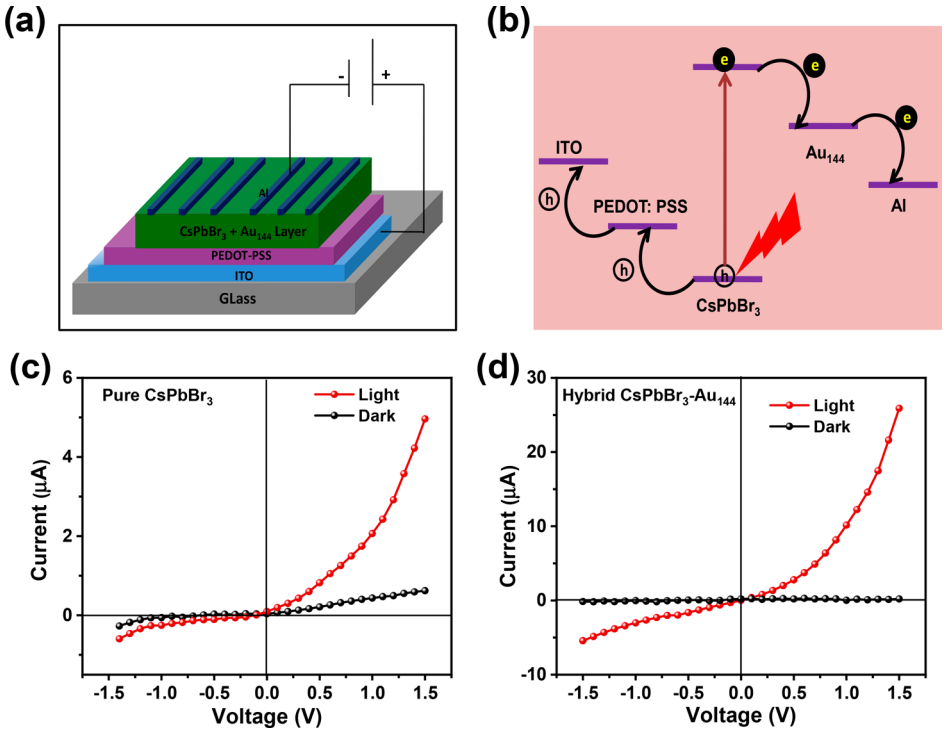

Figure 5. (a) Schematic representation of the device architecture and (b) schematic diagram of the charge separation mechanism of hybrid $CsPbBr_3$-Au_{144} system. $I-V$ characteristics curve of (c) pure $CsPbBr_3$ nanocrystals and (d) hybrid $CsPbBr_3$-Au_{144} system at a fixed bias voltage of 1.5 V.

with the following the Maxwell–Boltzmann (MB) distribution function:[12,16]

$$\Delta T(\hbar\omega) = -T_0 \exp\left(\frac{E_F - \hbar\omega}{k_B T_C}\right) \quad (4)$$

where ΔT indicates the amplitude of bleach at a particular probe wavelength, T_C, E_F, and k_B are the HC temperature, quasi-Fermi energy level, and Boltzmann constant, respectively. Here, we have measured the T_C after 450 fs to ensure that a quasi-equilibrium state is attained by HCs. MB fitting regions are indicated by the shaded portion (2.51–2.70 eV) in Figure 4a and b. It is to be noted that T_C signifies an average of both electron and hole distribution temperatures.[14] Figure 4c presents the comparison of time-dependent decay of T_C of pure $CsPbBr_3$ nanocrystals and hybrid $CsPbBr_3$-Au_{144}, and a faster relaxation rate in hybrid systems is concluded. The obtained initial T_C (after 450 fs) is 1055 ± 30 and 860 ± 25 K for pure $CsPbBr_3$ nanocrystals and hybrid $CsPbBr_3$-Au_{144}, respectively. Additionally, the relaxation time of T_C to reach T_L (370 K) is much faster for hybrid $CsPbBr_3$-Au_{144} (~1.1 ps) as compared to pure $CsPbBr_3$ nanocrystals (~1.8 ps). The reduction of initial T_C and faster decay time confirm the HC transfer occurs in the hybrid systems.

Photocurrent Measurement

To understand the charge separation via charge transfer, we have also measured the photocurrent for the devices with pure $CsPbBr_3$ nanocrystals and hybrid $CsPbBr_3$-Au_{144} as absorber layers, under the illumination of light using a 300 W xenon lamp without any wavelength cutoff filter by varying the scanning voltage up to 1.5 V. Figure 5a represents the device architecture of the sample schematically. Figure 5b provides information about the charge separation mechanism in the fabricated devices. According to the band alignment diagram of the pure $CsPbBr_3$ nanocrystals and pure Au_{144} NCs, the photoexcited electrons of the nanocrystals transferred to the CB of Au_{144} NCs which is further collected by Al electrodes, and the photoexcited holes of the $CsPbBr_3$ nanocrystals are transported in the reverse direction toward ITO electrode via PEDOT:PSS. Here, Figure 5c and d presents the typical $I-V$ characteristics of pure $CsPbBr_3$ nanocrystals and hybrid $CsPbBr_3$-Au_{144} with and without light illumination, respectively. The obtained dark current and photocurrent of pure $CsPbBr_3$ nanocrystals are found to be 0.62 and 4.96 μA, respectively, under a bias of 1.5 V, and the ratio of I_L and I_D (I_L and I_D are the photocurrent in the presence and absence of light, respectively) is 8.1 for pure $CsPbBr_3$ nanocrystals. Interestingly, we have obtained a significantly enhanced photocurrent (~25.9 μA) and the ratio of I_L and I_D was observed at ~123 for the hybrid $CsPbBr_3$-Au_{144} system. The hybrid $CsPbBr_3$-Au_{144} systems have exhibited a much higher ratio of I_L and I_D compared to that of pure $CsPbBr_3$ nanocrystals. So, the dramatically enhanced photocurrent and the improved ratio of I_L and I_D in the hybrid confirms their efficient charge separation because of the ultrafast electron-transfer process in the presence of Au_{144} NCs.

CONCLUSION

We have demonstrated the ultrafast electron dynamics in the Au_{144}-based hybrid $CsPbBr_3$ nanocrystals using TA spectroscopy. TA analysis reveals that the reduction of HC cooling time and the significant drop in T_C, confirming the transfer of hot electrons from $CsPbBr_3$ nanocrystals to Au_{144} NCs. A two times faster hot electron transfer rate is observed compared to the band-edge electron transfer rate and 45% hot-electron transfer efficiency is concluded in the hybrid system. The

https://doi.org/10.1021/acsphyschemau.2c00070
ACS Phys. Chem Au 2023, 3, 348–357

enhancement of photocurrent and a higher ratio of photocurrent to dark current in the hybrid system confirms the charge separation via electron transfer, followed by carrier extraction from $CsPbBr_3$ nanocrystals. Our findings point out the significance of metal cluster-based hybrid $CsPbBr_3$ nanocrystals to utilize the excess energy of LHPs nanocrystals and would be beneficial for optoelectronic applications.

■ ASSOCIATED CONTENT

Supporting Information

The Supporting Information is available free of charge at https://pubs.acs.org/doi/10.1021/acsphyschemau.2c00070.

MALDI-Mass spectra of Au_{144} NCs, TEM images of hybrid, XRD patterns, UV−visible absorption and PL spectra of samples, TCSPC table, CV curves of Au_{144} NCs, TA spectra of nanocrystals, TA spectra of pure Au_{144} NCs, PIA and GSB spectra, EAS spectra, details of extraction of HC cooling time from TA spectra by global fitting, fitted decay parameter of TA spectra, PLE spectra, comparison of absolute bleach amplitude (PDF)

■ AUTHOR INFORMATION

Corresponding Author

Amitava Patra − *School of Materials Sciences, Indian Association for the Cultivation of Science, Jadavpur, Kolkata 700032, India; Institute of Nano Science and Technology, Mohali 140306, India;* orcid.org/0000-0002-8996-9015; Phone: (91)-33-2473-4971; Email: msap@iacs.res.in; Fax: (91)-33-2473-2805

Authors

Kritiman Marjit − *School of Materials Sciences, Indian Association for the Cultivation of Science, Jadavpur, Kolkata 700032, India;* orcid.org/0000-0002-0049-8932

Goutam Ghosh − *School of Materials Sciences, Indian Association for the Cultivation of Science, Jadavpur, Kolkata 700032, India;* orcid.org/0000-0003-1912-5121

Srijon Ghosh − *School of Materials Sciences, Indian Association for the Cultivation of Science, Jadavpur, Kolkata 700032, India;* orcid.org/0000-0002-2056-2532

Debarati Ghosh − *School of Materials Sciences, Indian Association for the Cultivation of Science, Jadavpur, Kolkata 700032, India;* orcid.org/0000-0002-3086-7751

Anusri Medda − *School of Materials Sciences, Indian Association for the Cultivation of Science, Jadavpur, Kolkata 700032, India;* orcid.org/0000-0002-8682-7396

Complete contact information is available at: https://pubs.acs.org/10.1021/acsphyschemau.2c00070

Notes

The authors declare no competing financial interest.

■ ACKNOWLEDGMENTS

"DST-TRC" is gratefully acknowledged for financial support. K.M., S.G., and D.G. thank CSIR for awarding fellowships. G.G. acknowledges IACS for fellowship. A.M. thanks UGC for the fellowships.

■ REFERENCES

(1) Zhou, H.; Chen, Q.; Li, G.; Luo, S.; Song, T.-b.; Duan, H.-S.; Hong, Z.; You, J.; Liu, Y.; Yang, Y. Interface Engineering of Highly Efficient Perovskite Solar Cells. *Science* **2014**, *345*, 542−546.

(2) Kojima, A.; Teshima, K.; Shirai, Y.; Miyasaka, T. Organometal Halide Perovskites as Visible-Light Sensitizers for Photovoltaic Cells. *J. Am. Chem. Soc.* **2009**, *131*, 6050−6051.

(3) Kambhampati, P. Multiexcitons in Semiconductor Nanocrystals: A Platform for Optoelectronics at High Carrier Concentration. *J. Phys. Chem. Lett.* **2012**, *3*, 1182−1190.

(4) Saidaminov, M. I.; Adinolfi, V.; Comin, R.; Abdelhady, A. L.; Peng, W.; Dursun, I.; Yuan, M.; Hoogland, S.; Sargent, E. H.; Bakr, O. M. Planar-Integrated Single-Crystalline Perovskite Photodetectors. *Nat. Commun.* **2015**, *6*, 8724.

(5) Xiao, Z.; Kerner, R. A.; Zhao, L.; Tran, N. L.; Lee, K. M.; Koh, T.-W.; Scholes, G. D.; Rand, B. P. Efficient Perovskite Light-Emitting Diodes Featuring Nanometre-Sized Crystallites. *Nat. Photonics* **2017**, *11*, 108−115.

(6) Protesescu, L.; Yakunin, S.; Bodnarchuk, M. I.; Krieg, F.; Caputo, R.; Hendon, C. H.; Yang, R. X.; Walsh, A.; Kovalenko, M. V. Nanocrystals of Cesium Lead Halide Perovskites ($CsPbX_3$, X = Cl, Br, and I): Novel Optoelectronic Materials Showing Bright Emission with Wide Color Gamut. *Nano Lett.* **2015**, *15*, 3692−3696.

(7) Stranks, S. D.; Eperon, G. E.; Grancini, G.; Menelaou, C.; Alcocer, M. J. P.; Leijtens, T.; Herz, L. M.; Petrozza, A.; Snaith, H. J. Electron-Hole Diffusion Lengths Exceeding 1 Micrometer in an Organometal Trihalide Perovskite Absorber. *Science* **2013**, *342*, 341−344.

(8) Huang, H.; Bodnarchuk, M. I.; Kershaw, S. V.; Kovalenko, M. V.; Rogach, A. L. Lead Halide Perovskite Nanocrystals in the Research Spotlight: Stability and Defect Tolerance. *ACS Energy Lett.* **2017**, *2*, 2071−2083.

(9) De Roo, J.; Ibáñez, M.; Geiregat, P.; Nedelcu, G.; Walravens, W.; Maes, J.; Martins, J. C.; Van Driessche, I.; Kovalenko, M. V.; Hens, Z. Highly Dynamic Ligand Binding and Light Absorption Coefficient of Cesium Lead Bromide Perovskite Nanocrystals. *ACS Nano* **2016**, *10*, 2071−2081.

(10) Li, M.; Fu, J.; Xu, Q.; Sum, T. C. Slow Hot-Carrier Cooling in Halide Perovskites: Prospects for Hot-Carrier Solar Cells. *Adv. Mater.* **2019**, *31*, 1802486.

(11) Kahmann, S.; Loi, M. A. Hot Carrier Solar Cells and the Potential of Perovskites for Breaking the Shockley-Queisser Limit. *J. Mater. Chem. C* **2019**, *7*, 2471−2486.

(12) Marjit, K.; Ghosh, G.; Biswas, R. K.; Ghosh, S.; Pati, S. K.; Patra, A. Modulating the Carrier Relaxation Dynamics in Heterovalently (Bi^{3+}) Doped $CsPbBr_3$ Nanocrystals. *J. Phys. Chem. Lett.* **2022**, *13*, 5431−5440.

(13) Manley, M. E.; Hong, K.; Yin, P.; Chi, S.; Cai, Y.; Hua, C.; Daemen, L. L.; Hermann, R. P.; Wang, H.; May, A. F.; et al. Giant Isotope Effect on Phonon Dispersion and Thermal Conductivity in Methylammonium Lead Iodide. *Sci. Adv.* **2020**, *6*, eaaz1842.

(14) Nie, Z.; Gao, X.; Ren, Y.; Xia, S.; Wang, Y.; Shi, Y.; Zhao, J.; Wang, Y. Harnessing Hot Phonon Bottleneck in Metal Halide Perovskite Nanocrystals via Interfacial Electron-Phonon Coupling. *Nano Lett.* **2020**, *20*, 4610−4617.

(15) Shockley, W.; Queisser, H. J. Detailed Balance Limit of Efficiency of p-n Junction Solar Cells. *J. Appl. Phys.* **1961**, *32*, 510−519.

(16) Ghosh, G.; Biswas, R. K.; Marjit, K.; Ghosh, S.; Ghosh, A.; Pati, S. K.; Patra, A. Impacts of $CsPbBr_3$/PbSe Heterostructures on Carrier Cooling Dynamics at Low Carrier Density. *Adv. Opt. Mater.* **2022**, *10*, 2200030.

(17) Cooney, R. R.; Sewall, S. L.; Anderson, K. E. H.; Dias, E. A.; Kambhampati, P. Breaking the Phonon Bottleneck for Holes in Semiconductor Quantum Dots. *Phys. Rev. Lett.* **2007**, *98*, 177403.

(18) Yang, Y.; Ostrowski, D. P.; France, R. M.; Zhu, K.; van de Lagemaat, J.; Luther, J. M.; Beard, M. C. Observation of a Hot-Phonon Bottleneck in Lead-Iodide Perovskites. *Nat. Photonics* **2016**, *10*, 53−59.

(19) Manser, J. S.; Kamat, P. V. Band Filling with Free Charge Carriers in Organometal Halide Perovskites. *Nat. Photonics* **2014**, *8*, 737−743.
(20) Fu, J.; Xu, Q.; Han, G.; Wu, B.; Huan, C. H. A.; Leek, M. L.; Sum, T. C. Hot Carrier Cooling Mechanisms in Halide Perovskites. *Nat. Commun.* **2017**, *8*, 1300.
(21) Xing, G.; Mathews, N.; Sun, S.; Lim, S. S.; Lam, Y. M.; Grätzel, M.; Mhaisalkar, S.; Sum, T. C. Long-Range Balanced Electron and Hole-Transport Lengths in Organic-Inorganic $CH_3NH_3PbI_3$. *Science* **2013**, *342*, 344−347.
(22) Sun, Q.; Gong, J.; Yan, X.; Wu, Y.; Cui, R.; Tian, W.; Jin, S.; Wang, Y. Elucidating the Unique Hot Carrier Cooling in Two-Dimensional Inorganic Halide Perovskites: The Role of Out-of-Plane Carrier-Phonon Coupling. *Nano Lett.* **2022**, *22*, 2995−3002.
(23) Wei, Q.; Yin, J.; Bakr, O. M.; Wang, Z.; Wang, C.; Mohammed, O. F.; Li, M.; Xing, G. Effect of Zinc-Doping on the Reduction of the Hot-Carrier Cooling Rate in Halide Perovskites. *Angew. Chem., Int. Ed.* **2021**, *60*, 10957−10963.
(24) Chen, J.; Messing, M. E.; Zheng, K.; Pullerits, T. Cation-Dependent Hot Carrier Cooling in Halide Perovskite Nanocrystals. *J. Am. Chem. Soc.* **2019**, *141*, 3532−3540.
(25) Li, M.; Bhaumik, S.; Goh, T. W.; Kumar, M. S.; Yantara, N.; Grätzel, M.; Mhaisalkar, S.; Mathews, N.; Sum, T. C. Slow Cooling and Highly Efficient Extraction of Hot Carriers in Colloidal Perovskite Nanocrystals. *Nat. Commun.* **2017**, *8*, 14350.
(26) Ghosh, G.; Marjit, K.; Ghosh, S.; Ghosh, A.; Ahammed, R.; De Sarkar, A.; Patra, A. Hot Hole Cooling and Transfer Dynamics from Lead Halide Perovskite Nanocrystals Using Porphyrin Molecules. *J. Phys. Chem. C* **2021**, *125*, 5859−5869.
(27) Dursun, I.; Maity, P.; Yin, J.; Turedi, B.; Zhumekenov, A. A.; Lee, K. J.; Mohammed, O. F.; Bakr, O. M. Why are Hot Holes Easier to Extract than Hot Electrons from Methylammonium Lead Iodide Perovskite? *Adv. Energy Mater.* **2019**, *9*, 1900084.
(28) Li, X.; Li, W.; Yang, Y.; Lai, X.; Su, Q.; Wu, D.; Li, G.; Wang, K.; Chen, S.; Sun, X. W.; et al. Defects Passivation With Dithienobenzodithiophene-based π-conjugated Polymer for Enhanced Performance of Perovskite Solar Cells. *Sol. RRL* **2019**, *3*, 1900029.
(29) Kim, B.; Kim, M.; Kim, H.; Jeong, S.; Yang, J.; Jeong, M. S. Improved Stability of $MAPbI_3$ Perovskite Solar Cells Using Two-Dimensional Transition-Metal Dichalcogenide Interlayers. *ACS Appl. Mater. Interfaces* **2022**, *14*, 35726−35733.
(30) Ghosh, G.; Marjit, K.; Ghosh, S.; Ghosh, D.; Patra, A. Evidence of Hot Charge Carrier Transfer in Hybrid $CsPbBr_3$/Functionalized Graphene. *ChemNanoMat* **2022**, *8*, e202200172.
(31) Shen, Q.; Ripolles, T. S.; Even, J.; Zhang, Y.; Ding, C.; Liu, F.; Izuishi, T.; Nakazawa, N.; Toyoda, T.; Ogomi, Y.; et al. Ultrafast Selective Extraction of Hot Holes from Cesium Lead Iodide Perovskite Films. *J. Energy Chem.* **2018**, *27*, 1170−1174.
(32) Jin, R.; Zeng, C.; Zhou, M.; Chen, Y. Atomically Precise Colloidal Metal Nanoclusters and Nanoparticles: Fundamentals and Opportunities. *Chem. Rev.* **2016**, *116*, 10346−10413.
(33) Maity, S.; Bain, D.; Patra, A. An Overview on the Current Understanding of the Photophysical Properties of Metal Nanoclusters and their Potential Applications. *Nanoscale* **2019**, *11*, 22685−22723.
(34) Pyo, K.; Thanthirige, V. D.; Yoon, S. Y.; Ramakrishna, G.; Lee, D. Enhanced Luminescence of $Au_{22}(SG)_{18}$ Nanoclusters via Rational Surface Engineering. *Nanoscale* **2016**, *8*, 20008−20016.
(35) Bain, D.; Paramanik, B.; Sadhu, S.; Patra, A. A Study into the Role of Surface Capping on Energy Transfer in Metal Cluster-Semiconductor Nanocomposites. *Nanoscale* **2015**, *7*, 20697−20708.
(36) Mondal, N.; Paul, S.; Samanta, A. Photoinduced 2-Way Electron Transfer in Composites of Metal Nanoclusters and Semiconductor Quantum Dots. *Nanoscale* **2016**, *8*, 14250−14256.
(37) Maity, S.; Bain, D.; Bhattacharyya, K.; Das, S.; Bera, R.; Jana, B.; Paramanik, B.; Datta, A.; Patra, A. Ultrafast Relaxation Dynamics of Luminescent Copper Nanoclusters (Cu_7L_3) and Efficient Electron Transfer to Functionalized Reduced Graphene Oxide. *J. Phys. Chem. C* **2018**, *122*, 13354−13362.
(38) Medda, A.; Dutta, A.; Bain, D.; Mohanta, M. K.; De Sarkar, A.; Patra, A. Electronic Structure Modulation of 2D Colloidal CdSe Nanoplatelets by Au_{25} Clusters for High-Performance Photodetectors. *J. Phys. Chem. C* **2020**, *124*, 19793−19801.
(39) Malola, S.; Lehtovaara, L.; Enkovaara, J.; Häkkinen, H. Birth of the Localized Surface Plasmon Resonance in Monolayer-Protected Gold Nanoclusters. *ACS Nano* **2013**, *7*, 10263−10270.
(40) Dainese, T.; Agrachev, M.; Antonello, S.; Badocco, D.; Black, D. M.; Fortunelli, A.; Gascón, J. A.; Stener, M.; Venzo, A.; Whetten, R. L.; et al. Atomically Precise $Au_{144}(SR)_{60}$ Nanoclusters (R = Et, Pr) are Capped by 12 Distinct Ligand Types of 5-fold Equivalence and Display Gigantic Diastereotopic Effects. *Chem. Sci.* **2018**, *9*, 8796−8805.
(41) Yi, C.; Tofanelli, M. A.; Ackerson, C. J.; Knappenberger, K. L., Jr Optical Properties and Electronic Energy Relaxation of Metallic $Au_{144}(SR)_{60}$ Nanoclusters. *J. Am. Chem. Soc.* **2013**, *135*, 18222−18228.
(42) Qian, H.; Jin, R. Ambient Synthesis of $Au_{144}(SR)_{60}$ Nanoclusters in Methanol. *Chem. Mater.* **2011**, *23*, 2209−2217.
(43) Ghosh, S.; Chakraborty, S.; Ghosh, A.; Marjit, K.; Ghosh, G.; Patra, A. Ultrafast Relaxation Dynamics of Conjugated Polymer Nanoparticles by Tuning Their Interchain Interactions. *J. Phys. Chem. C* **2022**, *126*, 18177−18187.
(44) Ghosh, S.; Ghosh, A.; Ghosh, G.; Marjit, K.; Patra, A. Deciphering the Relaxation Mechanism of Red-Emitting Carbon Dots Using Ultrafast Spectroscopy and Global Target Analysis. *J. Phys. Chem. Lett.* **2021**, *12*, 8080−8087.
(45) Ghosh, G.; Dutta, A.; Ghosh, A.; Ghosh, S.; Patra, A. Ultrafast Carrier Dynamics in 2D CdSe Nanoplatelets-$CsPbX_3$ Composites: Influence of the Halide Composition. *J. Phys. Chem. C* **2020**, *124*, 10252−10260.
(46) Butkus, J.; Vashishtha, P.; Chen, K.; Gallaher, J. K.; Prasad, S. K. K.; Metin, D. Z.; Laufersky, G.; Gaston, N.; Halpert, J. E.; Hodgkiss, J. M. The Evolution of Quantum Confinement in $CsPbBr_3$ Perovskite Nanocrystals. *Chem. Mater.* **2017**, *29*, 3644−3652.
(47) Zhang, W.; Kong, J.; Li, Y.; Kuang, Z.; Wang, H.; Zhou, M. Coherent Vibrational Dynamics of $Au_{144}(SR)_{60}$ Nanoclusters. *Chem. Sci.* **2022**, *13*, 8124−8130.
(48) Ghosh, G.; Jana, B.; Sain, S.; Ghosh, A.; Patra, A. Influence of Shape on the Carrier Relaxation Dynamics of $CsPbBr_3$ Perovskite Nanocrystals. *Phys. Chem. Chem. Phys.* **2019**, *21*, 19318−19326.
(49) Koscher, B. A.; Swabeck, J. K.; Bronstein, N. D.; Alivisatos, A. P. Essentially Trap-Free $CsPbBr_3$ Colloidal Nanocrystals by Postsynthetic Thiocyanate Surface Treatment. *J. Am. Chem. Soc.* **2017**, *139*, 6566−6569.
(50) Ravi, V. K.; Markad, G. B.; Nag, A. Band Edge Energies and Excitonic Transition Probabilities of Colloidal $CsPbX_3$ (X = Cl, Br, I) Perovskite Nanocrystals. *ACS Energy Lett.* **2016**, *1*, 665−671.
(51) Marjit, K.; Ghosh, G.; Ghosh, S.; Sain, S.; Ghosh, A.; Patra, A. Structural Analysis and Carrier Relaxation Dynamics of 2D $CsPbBr_3$ Nanoplatelets. *J. Phys. Chem. C* **2021**, *125*, 12214−12223.
(52) Palato, S.; Seiler, H.; Baker, H.; Sonnichsen, C.; Brosseau, P.; Kambhampati, P. Investigating the Electronic Structure of Confined Multiexcitons with Nonlinear Spectroscopies. *J. Chem. Phys.* **2020**, *152*, 104710.
(53) Mondal, N.; De, A.; Das, S.; Paul, S.; Samanta, A. Ultrafast Carrier Dynamics of Metal Halide Perovskite Nanocrystals and Perovskite-Composites. *Nanoscale* **2019**, *11*, 9796−9818.
(54) Saran, R.; Heuer-Jungemann, A.; Kanaras, A. G.; Curry, R. J. Giant Bandgap Renormalization and Exciton-Phonon Scattering in Perovskite Nanocrystals. *Adv. Opt. Mater.* **2017**, *5*, 1700231.
(55) Sewall, S. L.; Cooney, R. R.; Dias, E. A.; Tyagi, P.; Kambhampati, P. State-resolved Observation in Real Time of the Structural Dynamics of Multiexcitons in Semiconductor Nanocrystals. *Phys. Rev. B* **2011**, *84*, 235304.
(56) Sewall, S. L.; Cooney, R. R.; Anderson, K. E. H.; Dias, E. A.; Sagar, D. M.; Kambhampati, P. State-resolved Studies of Biexcitons and Surface Trapping Dynamics in Semiconductor Quantum Dots. *J. Chem. Phys.* **2008**, *129*, 084701.

https://doi.org/10.1021/acsphyschemau.2c00070
ACS Phys. Chem Au 2023, 3, 348−357

(57) Chung, H.; Jung, S. I.; Kim, H. J.; Cha, W.; Sim, E.; Kim, D.; Koh, W.-K.; Kim, J. Composition-Dependent Hot Carrier Relaxation Dynamics in Cesium Lead Halide ($CsPbX_3$, X = Br and I) Perovskite Nanocrystals. *Angew. Chem., Int. Ed.* **2017**, *56*, 4160−4164.
(58) Ghosh, D.; Marjit, K.; Ghosh, G.; Ghosh, S.; Patra, A. Charge Transfer Dynamics of Two-Dimensional Ruddlesden Popper Perovskite in the Presence of Short-Chain Aromatic Thiol Ligands. *J. Phys. Chem. C* **2022**, *126*, 14590−14597.
(59) Wu, K.; Liang, G.; Shang, Q.; Ren, Y.; Kong, D.; Lian, T. Ultrafast Interfacial Electron and Hole Transfer from $CsPbBr_3$ Perovskite Quantum Dots. *J. Am. Chem. Soc.* **2015**, *137*, 12792−12795.
(60) Richter, J. M.; Branchi, F.; Valduga de Almeida Camargo, F.; Zhao, B.; Friend, R. H.; Cerullo, G.; Deschler, F. Ultrafast Carrier Thermalization in Lead Iodide Perovskite Probed with Two-Dimensional Electronic Spectroscopy. *Nat. Commun.* **2017**, *8*, 376.

https://doi.org/10.1021/acsphyschemau.2c00070
ACS Phys. Chem Au 2023, 3, 348−357